INORGANIC CHEMISTRY
FRONTIERS

RESEARCH ARTICLE

View Article Online
View Journal | View Issue

Cite this: *Inorg. Chem. Front.*, 2022, **9**, 1847

Phosphorus doped two-dimensional $CoFe_2O_4$ nanobelts decorated with Ru nanoclusters and Co–Fe hydroxide as efficient electrocatalysts toward hydrogen generation†

Wenli Yu,[a] Zhi Chen,[b] Weiping Xiao,[c] Yongming Chai,[a] Bin Dong,* [a] Zexing Wu *[b,d] and Lei Wang [b]

Developing efficient and durable hydrogen evolution reaction (HER) electrocatalysts has attracted considerable attention for large-scale hydrogen generation. In this work, phosphorus doped two-dimensional (2D) $CoFe_2O_4$ nanobelts decorated with Ru and CoFe hydroxide clusters on iron foam (IF) ($CoFeO_xH_y$–Ru/P–$CoFe_2O_4$/IF) are synthesized *via* a solvothermal method followed by phosphorization procedures. The specific nanobelt morphology favors the exposure of active sites, advantageous electron transportation and intimate contact between the electrolyte and electrocatalyst. Interestingly, abundant metal hydroxide nanosheets are *in situ* generated on the nanobelt after the phosphorized sample is immersed in an alkaline electrolyte. Benefiting from the above merits, the developed $CoFeO_xH_y$–Ru/P–$CoFe_2O_4$/IF presents excellent electrocatalytic performances for the HER with low overpotentials of 38.6 mV, 43.2 mV, and 30.1 mV to attain 50 mA cm^{-2} and 54.4 mV, 71.5 mV, and 69.3 mV to attain 100 mA cm^{-2} in 1 M KOH, 1 M KOH seawater and 1 M PBS, respectively. As for overall water splitting, a cell voltage as low as 1.49 V is necessary to attain 10 mA cm^{-2} and the developed $CoFeO_xH_y$–Ru/P–$CoFe_2O_4$/IF also exhibits excellent long-term stability. This work provides a new avenue for designing efficient HER catalysts with high exposure of precious metals.

Received 11th January 2022,
Accepted 5th March 2022

DOI: 10.1039/d2qi00086e

rsc.li/frontiers-inorganic

1. Introduction

It is of importance to exploit sustainable and green energies to alleviate the ever-increasing environmental contamination and energy crisis.[1–4] Among them, hydrogen, a high energy density and eco-friendly energy carrier, is identified as a promising energy storage medium to solve the issues of intermittent sustainable energies, such as solar, wind and ocean energies.[5–9] Electrocatalytic overall water-splitting has been considered the most eco-friendly and desired means to produce hydrogen without the generation of pollutant gases in comparison with the traditional synthetic technologies.[10–13] Therefore, it is crucial to utilize catalysts to expedite the HER to achieve high electrocatalytic performance.[14–19] So far, Pt-based nanomaterials are deemed to be the most efficient electrocatalysts for the HER with the most favorable reaction kinetics.[20,21] Nevertheless, their scarcity and high cost limited their further large-scale implementation for hydrogen generation.[22–24] Thus, tremendous efforts have been devoted to settle the challenges of exploring efficient and Pt-free catalysts for the HER.[25–28]

More recently, Ru-based electrocatalysts have been investigated extensively to substitute Pt for the HER due to their low cost, excellent electrocatalytic performance and remarkable stability.[29,30] For example, Liu *et al.* reported phosphatized Ru–Fe bimetallic nanoclusters (Ru_xFe_yP-NCs) dispersed on graphitized carbon nanofiber (CNF) supports with low overpotentials of 65.8 and 16.0 mV at 10 mA cm^{-2} in acidic and alkaline media with an excellent stability of 100 h for the HER.[31] In general, a high content of Ru is necessary to drive the excellent electrocatalytic performance which then increases the cost of hydrogen energy. It is widely recognized that decreasing the particle size is a valid strategy to improve the electrocatalytic activity by exposing abundant active sites.[32–34] Moreover, the

[a]*State Key Laboratory of Heavy Oil Processing, College of Science, China University of Petroleum (East China), Qingdao, 266580, P. R. China. E-mail: dongbin@upc.edu.cn, ymchai@upc.edu.cn*
[b]*Key Laboratory of Eco-chemical Engineering, Taishan Scholar Advantage and Characteristic Discipline Team of Eco Chemical Process and Technology, Ministry of Education, Laboratory of Inorganic Synthesis and Applied Chemistry, College of Chemistry and Molecular Engineering, Qingdao University of Science and Technology, Qingdao 266042, P. R. China. E-mail: splswzx@qust.edu.cn*
[c]*College of Science, Nanjing Forestry University, Nanjing, 210037, PR China*
[d]*Key Laboratory of Advanced Energy Materials Chemistry (Ministry of Education), College of Chemistry, Nankai University, Tianjin 300071, China*
† Electronic supplementary information (ESI) available: SEM images, XRD patterns, XPS spectra, electrochemical data. See DOI: 10.1039/d2qi00086e

morphology of the designed electrocatalysts also plays a pivotal role in regulating the electrocatalytic performance.[35,36] Among the investigated nanostructures, the developed nanobelts possess particular merits, such as intimate contact between the catalyst and electrolyte, favorable electron and electrolyte transportation and the high exposure of active sites.[37] For instance, Zeng *et al.* synthesized silver doped cobalt selenide (Ag–$CoSe_2$) *via* a partial cation exchange strategy and the obtained electrocatalyst presented excellent electrocatalytic activity toward the OER.[38] Except the above-mentioned nanostructure regulation, heteroatom doping is also considered as a promising avenue to promote the electrocatalytic activity. Recently, Yu and co-authors demonstrated that the introduced N atom plays a significant role in improving the Ni–Mo based sulfide for the HER with small overpotentials of 68, 250, and 322 mV to attain 10, 500 and 1000 mA cm^{-2}, respectively.[39] Then, the combination of morphology regulation and heteroatom doping would be an attractive approach to optimize the electrocatalytic activity.

In this work, we designed P doped $CoFe_2O_4$ nanobelts decorated with Ru nanoclusters and Co–Fe hydroxides through hydrothermal and annealing treatment, followed by hydrolysis in an aqueous solution of potassium hydroxide (Scheme 1). The obtained specific nanobelt structure favors the exposure of active sites, provides rich catalytic sites and facilitates mass transport during the electrocatalytic process. The Ru species was introduced by dripping onto the substrate after the solvothermal process and then it can contact the electrolyte directly. Moreover, the Co–Fe hydroxide species were *in situ* generated on the nanobelts and played a significant role in promoting the electrocatalytic performance by tuning the adsorption/desorption of the intermediates. Owing to the above merits, the as-developed $CoFeO_xH_y$–Ru/P–$CoFe_2O_4$/IF presented remarkable electrocatalytic activities and long-term stability in various electrolytes.

2. Experimental section

2.1. Synthesis of Ru/P–$CoFe_2O_4$/IF

The IF (2.0 cm × 1.0 cm) was added into anhydrous ethanol, acetone, and anhydrous ethanol for 30 min under ultrasonic treatment to clean the surface impurities and then placed in a vacuum oven to dry overnight. After that, $Co(NO_3)_2{\cdot}6H_2O$ (0.3 g) and $Fe(NO_3)_2{\cdot}9H_2O$ (0.08 g) were dissolved in 15 mL H_2O under stirring to obtain a homogeneous solution. Then the solution was transferred into a 100 mL Teflon-lined stainless-steel autoclave with a piece of IF and heated at 120 °C for 7 h. After that, the black product was taken out and washed with absolute ethanol and deionized water to remove the unreacted materials. The standby solution was obtained by dissolving ruthenium chloride in anhydrous ethanol (0.116 M) and then dropping it onto the solvothermal product. Finally, 0.5 g of sodium hypophosphite and the reactant were placed upstream and downstream of a tube furnace for 2 h at 350 °C with a heating rate of 5 °C min^{-1}.

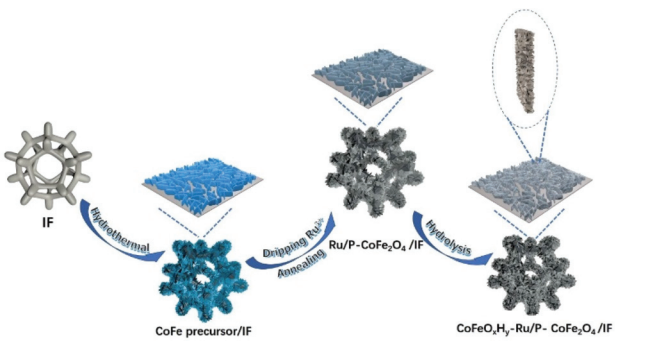

Scheme 1 Schematic illustration of the synthesis of $CoFeO_xH_y$–Ru/P–$CoFe_2O_4$/IF.

2.2. Synthesis of $CoFeO_xH_y$–Ru/P–$CoFe_2O_4$/IF

The synthesized precursor of Ru/P–$CoFe_2O_4$/IF was immersed in 1.0 M KOH for 3 h under constant stirring. The resulting electrode was denoted as $CoFeO_xH_y$–Ru/P–$CoFe_2O_4$/IF which could directly serve as the working electrode for subsequent electrochemical measurements. For comparison, $CoFeO_xH_y$/P–$CoFe_2O_4$ was prepared without ruthenium chloride addition. Other samples prepared with different amounts (50 mg and 100 mg) of $Fe(NO_3)_2{\cdot}9H_2O$ were named 50 mg–$Fe(NO_3)_2{\cdot}9H_2O$ and 100 mg–$Fe(NO_3)_2{\cdot}9H_2O$, respectively.

2.3. Synthesis of RuO_2/$CoFe_2O_4$

RuO_2/$CoFe_2O_4$ was obtained using a similar synthetic procedure to that of $CoFeO_xH_y$–Ru/P–$CoFe_2O_4$/IF, except pyrolysis in a muffle furnace at 380 °C for 2 h.

2.4. Physical characterization

The morphologies of the as-designed electrocatalysts were obtained by scanning electron microscopy (SEM) (Hitachi S-4800) and transmission electron microscopy (TEM) (FEI Tecni G20, 200 kV) analysis. Energy-dispersive X-ray spectroscopy (EDX) (FEI Tecni G20, 200 kV) was used to analyze the composition and distribution of elements in the samples. The crystal information was obtained by X-ray diffraction (XRD) (Rigaku D/max-2500pc device with Cu Kα radiation (λ = 1.54 Å)). The information about valence states of samples was obtained by X-ray photoelectron spectroscopy (XPS) carried out in a Thermo Fisher Scientific II spectrometer with an Al Kα source (1486.6 eV). The contents of Fe, Co and P were measured by inductively coupled plasma emission spectroscopy (ICP-OES) using an Agilent 720 instrument.

2.5. Electrochemical characterization

Electrochemical tests were performed *via* an electrochemical workstation (Gamry Reference 3000) with a typical three-electrode setup in solution (1.0 M KOH, seawater (1 M KOH), and 1 M PBS) at room temperature. The electrochemical measurements were carried out with a saturated calomel electrode (SCE) and graphite rod which were used as the reference electrode and counter electrode, respectively. All final potentials were given by E(RHE) = E(SCE) + E°(SCE) + 0.059 pH (E°(SCE) +

0.243 V). Linear sweep voltammetry (LSV) curves for the HER were determined with a scanning rate of 1 mV s^{-1}. EIS Nyquist plots for the obtained catalysts were obtained in a frequency range of 100 kHz–0.1 Hz at a potential of −1.15 V (*vs.* SCE) in 1 M KOH for the HER. Equivalent electrical circuit: R_s (R_1): solution resistance, CPE: constant phase element, R_{ct} (R_2): charge transfer resistance. Multiple-step chronopotentiometry was used to measure the long-term stability of all samples.

3. Results and discussion

The crystal structure of the as-designed $CoFeO_xH_y$–Ru/P–$CoFe_2O_4$/IF is composed of $CoFe_2O_4$ (PDF#00-002-1045) without other impurities. The microstructure of the synthesized electrocatalysts was investigated by SEM and TEM. As shown in Fig. S1,† relative to the smooth surface of iron foam without specific decorated nanomaterials, smooth nanobelts were generated after the solvothermal reaction (Fig. S2 and S3†). Obviously, the nanobelt nanostructure was maintained well after decoration with Ru and the phosphorization process (Fig. 1b and Fig. S4†). Interestingly, the smooth surface of the nanobelt was covered with numerous nanosheets after immersion in 1 M KOH (Fig. 1c). In order to verify the species of the nanosheets, Raman spectra were recorded before and after immersion in 1 M KOH. Evidently, new peaks, ascribed to metal hydroxide,[40] appeared after treatment with an alkaline solution, demonstrating the formation of Co–Fe hydroxide (Fig. S5†). On this basis, the electrocatalytic performances were recorded every 15 minutes (Fig. S6†). The catalytic activities improved with increasing soaking time and were well maintained after prolonged times, confirming that the generation of metal hydroxide plays a key role in regulating the catalytic performance. However, the smooth surface was retained well after soaking in deionized water, indicating that the hydroxide ion plays a pivotal role in forming metal hydroxide (Fig. S7†). The ICP-OES results (Table S1†) proved that the metal ions dissolved in the solution after soaking in 1 M KOH and then formed metal hydroxides. The nanosheets can be clearly observed by TEM and they are generated on the nanobelt homogeneously (Fig. 1d). As illustrated in Fig. 1e and f, Ru nanoclusters were decorated on the nanobelt homogenously with a lattice spacing of 0.206 nm of the (101) plane. Moreover, it can be observed in Fig. 1f that the interplanar spacings of 0.296 nm and 0.253 nm corresponded to the (200) and (311) facet of $CoFe_2O_4$, respectively. The elemental mappings confirmed that Co, Fe, P, O and Ru elements existed in the designed $CoFeO_xH_y$–Ru/P–$CoFe_2O_4$/IF (Fig. 1g and S8†). Moreover, for $CoFeO_xH_y$–Ru/P–$CoFe_2O_4$/IF, the BET surface area was 12.69 m^2 g^{-1} (Fig. S9†) with pore size distribution centers at 3.4 and 8.9 nm. The result confirms the mesoporous structure of the prepared catalysts which favours mass transport and exposure of abundant active sites during the electrocatalytic process.

XPS measurement was conducted to investigate the valence and composition of the as-prepared $CoFeO_xH_y$–Ru/P–$CoFe_2O_4$/IF. Obviously, P, O, Fe, Co, and Ru elements were detected from the XPS survey spectrum, which is in line with the EDS results. For high-resolution Co 2p (Fig. 2b), the peaks located at 782.3 eV and 780.7 eV are ascribed to Co^{2+} and Co^{3+}, respectively.[41–43] As illustrated in Fig. 2c, Fe^{2+} (710.5 eV) and Fe^{3+} (712.8 eV) are detected in the as-designed $CoFeO_xH_y$–Ru/P–$CoFe_2O_4$/IF.[44,45] For Ru 3p, the peak at a binding energy of 484.3 eV is assigned to Ru $3p_{1/2}$ and the adjacent peak at 462.2 eV corresponds to Ru $3p_{3/2}$ in the high-resolution Ru 3p XPS spectrum which confirmed that Ru was successfully incorporated.[31,46] The metal–oxide bond (531.6 eV, 530.8 eV and 529.7 eV) and the characteristic peaks of oxygen vacancies (530.8 eV) were obviously observed in the O 1s spectrum.[44] The P 2p in Fig. 2f demonstrates that P was doped into the prepared electrocatalyst successfully.[31,47–49] We investigated the XPS spectrum of Ru/P–$CoFe_2O_4$/IF and $CoFeO_xH_y$–Ru/P–$CoFe_2O_4$/IF to study the electronic interactions (Fig. S10†). For Co 2p, the peaks of $CoFeO_xH_y$–Ru/P–$CoFe_2O_4$/IF shift to a lower binding energy after the formation of CoFe–OH demonstrating that the electronic interactions play a pivotal role in

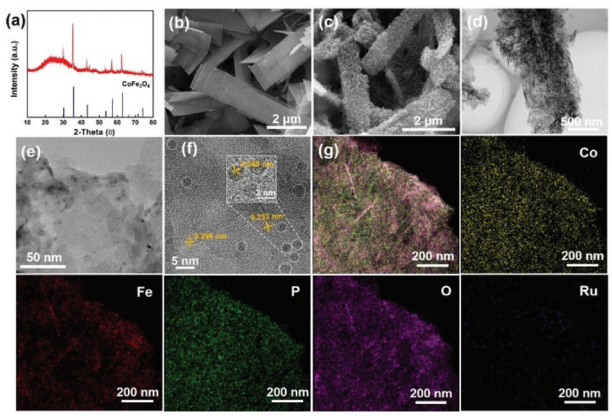

Fig. 1 (a) XRD patterns of $CoFeO_xH_y$–Ru/P–$CoFe_2O_4$/IF. SEM images of Ru/P–$CoFe_2O_4$/IF (b) and $CoFeO_xH_y$–Ru/P–$CoFe_2O_4$/IF (c). (d and e) TEM images of $CoFeO_xH_y$–Ru/P–$CoFe_2O_4$/IF. (f) HRTEM image of $CoFeO_xH_y$–Ru/P–$CoFe_2O_4$/IF. (g) Corresponding element mappings of Co, Fe, P, O, and Ru in $CoFeO_xH_y$–Ru/P–$CoFe_2O_4$/IF.

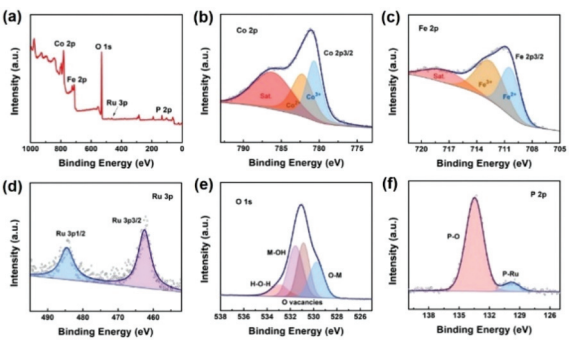

Fig. 2 XPS survey spectrum (a) and high-resolution XPS spectra of Co 2p (b), Fe 2p (c), Ru 3p (d), O 1s (e) and P 2p (f) of the designed $CoFeO_xH_y$–Ru/P–$CoFe_2O_4$/IF.

promoting the electrocatalytic performance. Besides, different peaks of Ru 3p shifted to a higher binding energy of $CoFeO_xH_y$–Ru/P–$CoFe_2O_4$/IF compared to that of Ru/P–$CoFe_2O_4$/IF further indicating electron transfer in the catalyst. It has been widely recognized in some research studies that the introduction of hydroxide can effectively improve the electrocatalytic activity.[50] Consequently, the formation of $CoFeO_xH_y$ will act as an electronic regulator leading to the redistribution of electrons, and finally the exhibition of outstanding HER activity by the sample.

The electrocatalytic HER performances of the as-designed $CoFeO_xH_y$–Ru/P–$CoFe_2O_4$/IF and reference samples were investigated in 1 M KOH *via* a typical three-electrode setup. Fig. 3a and b show the linear sweep voltammetry of $CoFeO_xH_y$–Ru/P–$CoFe_2O_4$/IF, $CoFeO_xH_y$–$CoFe_2O_4$/IF, Pt/C and IF. Remarkably, the designed $CoFeO_xH_y$–Ru/P–$CoFe_2O_4$/IF displays excellent HER activity with small overpotentials of 38.6 mV and 54.4 mV to attain 50 mA cm^{-2} and 100 mA cm^{-2}, respectively, compared with $CoFeO_xH_y$/P–$CoFe_2O_4$/IF (156 mV@10 mA cm^{-2}, 182 mV@100 mA cm^{-2}), indicating that the introduced Ru nanoclusters play key roles in improving the electrocatalytic performance. Ru clusters anchored on oxides with high conductivity play a key role in electron traps, and rapidly occupy electron and reduce H^+ to H_2. The intrinsic activity of the catalyst is significantly increased due to the synergistic effects of electron coupling between Ru and $CoFeO_xH_y$.[51] Besides, the Tafel plots demonstrated that $CoFeO_xH_y$–Ru/P–$CoFe_2O_4$/IF possesses a smaller value (43.2 mV dec^{-1}) than $CoFeO_xH_y$–$CoFe_2O_4$/IF (85.6 mV dec^{-1}), verifying its favorable reaction kinetics (Fig. 3c). The catalytic activity of the as-synthesized $CoFeO_xH_y$–Ru/P–$CoFe_2O_4$/IF surpasses most of the reported values (Fig. 3d and g and Tables S2 and S3†). As shown in Fig. S11,† $CoFeO_xH_y$–Ru/P–$CoFe_2O_4$/IF displays the smallest Nyquist semicircle diameter, demonstrating the lowest resistance of charge transfer during the electrocatalytic HER process.

In addition, the prepared composite catalyst contains dense and tiny hydroxide nanosheets relative to Ru/P–$CoFe_2O_4$/IF, which plays a pivotal role in boosting the catalytic process, and the specific nanostructure benefits the transport of the electrolyte and weakens the O–H bond in water. Despite the remarkable electrocatalytic performance, the developed $CoFeO_xH_y$–Ru/P–$CoFe_2O_4$/IF also possesses excellent long-term stability. As illustrated in Fig. 3e and f, the current densities increased when the applied potentials were increased, and the current densities were well maintained during the reverse process, indicating its outstanding stability. For an optimal performance, we investigated the role of the mass content of Fe $(NO_3)_2{\cdot}9H_2O$ in regulating the electrocatalytic activity for the HER (Fig. S12†). The results show that the electrocatalyst with 80 mg $Fe(NO_3)_2{\cdot}9H_2O$ exhibits the lowest overpotential and the smallest Tafel slope.

As mentioned above, the developed $CoFeO_xH_y$–Ru/P–$CoFe_2O_4$/IF exhibits excellent HER performance coupled with long-term stability. Then, we investigated its properties after the stability test by SEM and XPS measurements. As shown in Fig. 4a and b, the $CoFeO_xH_y$–Ru/P–$CoFe_2O_4$/IF maintained the nanobelt morphology covered with numerous Co–Fe hydroxides, demonstrating its robust structure. The XPS results (Fig. 4c–f and Fig. S13†) verify the elemental composition and the chemical valence shows negligible changes, verifying its stable property. Thus, all the tests confirmed the great potential of $CoFeO_xH_y$–Ru/P–$CoFe_2O_4$/IF as an effective electrocatalyst for practical hydrogen production.

The ocean covers nearly 71% of the Earth's surface area and seawater accounts for about 97% of the total water on the Earth. Seawater is inexhaustible for human beings, so the reasonable development of electrolytic seawater is very promising for hydrogen production.[52,53] As illustrated in Fig. 4a and b, the obtained electrocatalyst only needs low overpotentials of 43.2 mV and 71.5 mV to attain 50 mA cm^{-2} and 100 mA cm^{-2}, respectively (Fig. 5a and b). Relatively, the reference sample

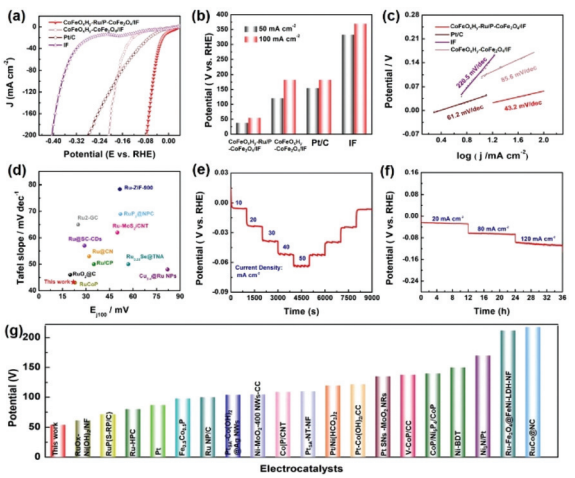

Fig. 3 Electrochemical measurements: (a) HER polarization curves. (b) Overpotential comparison at 50 mA cm^{-2} and 100 mA cm^{-2}. (c) Tafel slopes. (d) Comparison of the overpotentials and Tafel slopes with the references. (e and f) Stability tests of the obtained catalysts in 1 M KOH. (g) Comparison of the overpotentials (E_{j100}) with the reported electrocatalysts.

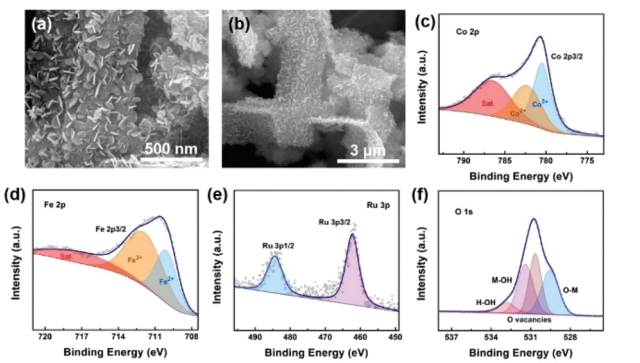

Fig. 4 (a and b) SEM images and XPS spectra of Co (c), Fe (d), Ru (e) and P (f) of the $CoFeO_xH_y$–Ru/P–$CoFe_2O_4$/IF after the long-term stability test.

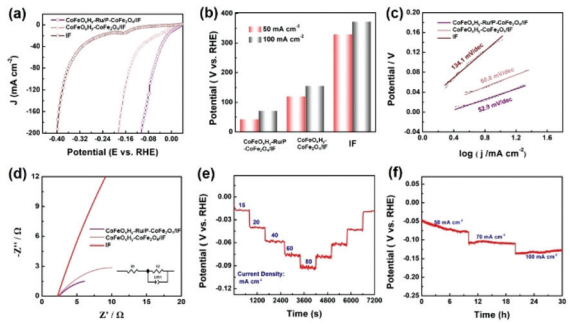

Fig. 5 Electrochemical measurements: (a) HER polarization curves. (b) Overpotential comparison at 50 mA cm^{-2} and 100 mA cm^{-2}. (c) Tafel slopes. (d) Nyquist plots. (e and f) Stability tests of the obtained catalysts in 1 M KOH seawater.

$CoFeO_xH_y$–$CoFe_2O_4$/IF needs 162 mV and IF needs 377 mV to deliver 100 mA cm^{-2}, respectively. Significantly, the synthesized $CoFeO_xH_y$–Ru/P–$CoFe_2O_4$/IF presented the lowest Tafel slope of 52.9 mV dec^{-1} compared with $CoFeO_xH_y$–$CoFe_2O_4$/IF (60.0 mV dec^{-1}) and IF (134.1 mV dec^{-1}), indicating its faster reaction kinetics for the HER (Fig. 5c). Fig. 5d shows the electrochemical impedance spectroscopy (EIS) results of the obtained catalysts in 1 M KOH seawater; the R_{ct} value of $CoFeO_xH_y$–Ru/P–$CoFe_2O_4$/IF is 9.65 Ω, lower than those of $CoFeO_xH_y$–$CoFe_2O_4$/IF (15.31 Ω) and IF (135.6 Ω). In addition, we also studied the stability of $CoFeO_xH_y$–Ru/P–$CoFe_2O_4$/IF in 1 M KOH seawater using an identical method in an alkaline medium. As shown in Fig. 5e and f, the durability measurement was confirmed by multiple-step chronopotentiometry with negligible decay as long as 30 h demonstrating its excellent stability in seawater.

Encouraged by the remarkable HER catalytic performance in alkaline media, the catalytic activity of $CoFeO_xH_y$–Ru/P–$CoFe_2O_4$/IF was further investigated in neutral medium (1 M PBS). As shown in Fig. 6a and b, the as-prepared $CoFeO_xH_y$–Ru/P–$CoFe_2O_4$/IF also possesses better catalytic activity than $CoFeO_xH_y$–$CoFe_2O_4$/IF and IF with the lowest overpotential of 30.1 mV and 69.3 mV to achieve current densities of 50 mA

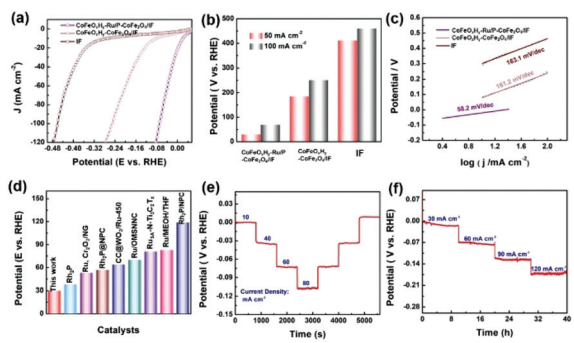

Fig. 6 Electrochemical measurements: (a) HER polarization curves. (b) Overpotential comparison at 50 mA cm^{-2} and 100 mA cm^{-2}. (c) Tafel slopes. (d) Comparison of the overpotentials with the references. (e and f) Stability tests of the obtained catalysts in 1 M PBS.

cm^{-2} and 100 mA cm^{-2}. Moreover, the Tafel slope of $CoFeO_xH_y$–Ru/P–$CoFe_2O_4$/IF (58.2 mV dec^{-1}) is lower than those of $CoFeO_xH_y$–$CoFe_2O_4$/IF (161.2 mV dec^{-1}) and IF (163.1 mV dec^{-1}) (Fig. 6c). The catalytic performance of $CoFeO_xH_y$–Ru/P–$CoFe_2O_4$/IF is even better than those of most of the reported noble metal catalysts, such as CC@WO_3/Ru-450 (64 mV),[54] Ru_{SA}–N–$Ti_3C_2T_x$ (81 mV),[55] Ru/OMSNNC (70 mV),[56] Rh_2P/NPC (119 mV),[57] Ru–Cr_2O_3/NG (53 mV),[58] Ru/MEOH/THF (83 mV),[59] Rh_2P (38 mV)[60] and RhP_2@NPC (57 mV)[61] (Fig. 6d and Table S4†). As shown in Fig. 6e and f, the as-prepared electrocatalyst presents excellent long-term stability in 1 M PBS.

Encouraged by the excellent electrocatalytic activity toward the HER, a two-electrode water-splitting setup was built with the prepared $CoFeO_xH_y$–Ru/P–$CoFe_2O_4$/IF as the cathode and RuO_2/$CoFe_2O_4$ (Fig. S14–S17†) as the anode for overall water-splitting in 1 M KOH solution (Fig. 7a). As shown in Fig. 7b, the electrolyzer can attain 10 mA cm^{-2} with a low voltage of 1.49 V which is lower than those of many other reported available catalysts (Fig. 7c and Table S5†).As solar energy is a sustainable and green energy, it attracts tremendous attention in hydrogen production. Thanks to the small voltage, the overall water-splitting setup is easily powered by solar energy then amounts of bubbles generated on the electrodes (Fig. 7d and Movie S1†). Importantly, the designed $CoFeO_xH_y$–Ru/P–$CoFe_2O_4$/IF||RuO_2/$CoFe_2O_4$ also exhibits excellent stability for overall water-splitting *via* multi-step measurements (Fig. 7e and f). As mentioned above, the developed electrocatalyst presents excellent catalytic activity which can be attributed to the following factors: the specific nanobelts favour the transport of the electrolyte; a trace amount of Ru nanoclusters plays a crucial role in improving the HER performance; and phosphorus can effectively optimize the density of electron clouds around metal atoms, resulting in an optimized hydrogen adsorption energy and favorable hydrogen release.[62] P atoms facilitate proton adsorption and thus accelerate the reaction

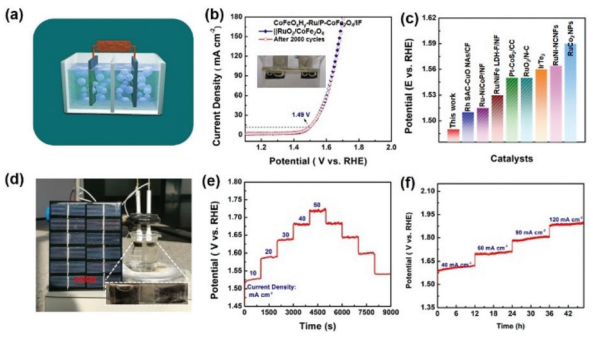

Fig. 7 (a) Schematic diagram of water splitting in a two-electrode setup. (b) LSV curves of $CoFeO_xH_y$–Ru/P–$CoFe_2O_4$/IF||RuO_2/$CoFe_2O_4$ and the catalyst after the stability test of 2000 cycles for overall water splitting in 1 M KOH (the inset is the photograph of the water splitting cell). (c) Solar cell driving overall water-splitting. (d) Comparison of the overpotentials (E_{j10}) of the synthesized electrocatalysts with the reported catalysts. (e and f) Stability tests of the obtained catalysts in 1 M KOH.

kinetics. In addition, the doped P can improve the electron mobility for attaining rapid electron transport, which can adjust the electron structure and play a role in regulating charge accumulation and consumption for an excellent HER.[63] Due to the different electronegativities of phosphorus, the catalytic activity of the composite components can be regulated, so that the obtained catalyst has good hydrogen evolution performance in 1 M KOH, 1 M KOH seawater and 1 M PBS; the *in situ* generated metal hydroxides play a key role in promoting the electrocatalytic performance by accelerating the reaction kinetics; the IF substrate provides abundant channels for the transport of the electrolyte and avoids the usage of a binding agent.

4. Conclusions

In summary, a hierarchical structure of $CoFeO_xH_y$–Ru/P–$CoFe_2O_4$/IF nanobelts decorated with dense and tiny CoFe double hydroxide nanosheets supported on iron foam is developed *via* hydrothermal and annealing treatment and further hydrolyzed in alkaline media. Owing to the combination of metal oxide species and a trace amount of Ru nanoclusters, in addition to the Co–Fe double hydroxide nanosheets during the hydrolysis process, the obtained composite nanomaterial serves as a remarkable electrocatalyst for boosting the HER activity in alkaline, seawater and neutral electrolytes. Accordingly, the obtained electrocatalyst exhibits excellent catalytic performances toward overall water-splitting with remarkable long-term stability in 1 M KOH, which can also be powered by sustainable solar energy. Additionally, the iron foam substrate possesses an intricate skeleton with rich channels which improves the electrical conductivity and timely release of the generated bubbles to expose the active substances. Ru clusters can accelerate the HER rate by converting into a faster electron transport paths and possess a moderate H* adsorption value in favour of the HER process. Consequently, the developed $CoFeO_xH_y$–Ru/P–$CoFe_2O_4$/IF presents superior performances to that of previously reported materials toward the HER and overall water-splitting. This work provides a valuable strategy to develop other specific nanostructures as efficient electrocatalysts for energy-related applications.

Conflicts of interest

There are no conflicts to declare.

Acknowledgements

The authors acknowledge funding support from the National Natural Science Foundation of China (22002068, 51772162, and 52072197), the Youth Innovation and Technology Foundation of Shandong Higher Education Institutions, China (2019KJC004), the Outstanding Youth Foundation of Shandong Province, China (ZR2019JQ14), the Taishan Scholar Young Talent Program (tsqn201909114), the Major Scientific and Technological Innovation Project (2019JZZY020405), the Major Basic Research Program of Natural Science Foundation of Shandong Province under Grant No. ZR2020ZD09, the Project funded by the China Postdoctoral Science Foundation (2021M691700), and the Natural Science Foundation of Shandong Province of China (ZR2019BB002 and ZR2018BB031).

Notes and references

1 L. Q. Gong, H. Yang, H. M. Wang, R. J. Qi, J. L. Wang, S. H. Chen, B. You, Z. H. Dong, H. F. Liu and B. Y. Xia, Corrosion formation and phase transformation of nickel-iron hydroxide nanosheets array for efficient water oxidation, *Nano Res.*, 2021, **14**, 4528–4533.
2 G. Zhao, W. Ma, X. Wang, Y. Xing, S. Hao and X. Xu, Self-water-absorption-type two-dimensional composite photocatalyst with high-efficiency water absorption and overall water-splitting performance, *Adv. Powder Mater.*, 2021, DOI: 10.1016/j.apmate.2021.09.008.
3 Z. Li, X. Wu, X. Jiang, B. Shen, Z. Teng, D. Sun, G. Fu and Y. Tang, Surface carbon layer controllable Ni_3Fe particles confined in hierarchical N-doped carbon framework boosting oxygen evolution reaction, *Adv. Powder Mater.*, 2022, DOI: 10.1016/j.apmate.2021.11.007.
4 J. Li, S. Zhang, J. Sha, H. Wang, M. Liu, L. Kong and G. Liu, Confined Molybdenum Phosphide in P-Doped Porous Carbon as Efficient Electrocatalysts for Hydrogen Evolution, *ACS Appl. Mater. Interfaces*, 2018, **10**, 17140–17146.
5 H. Yang, L. Gong, H. Wang, C. Dong, J. Wang, K. Qi, H. Liu, X. Guo and B. Xia, Preparation of nickel-iron hydroxides by microorganism corrosion for efficient oxygen evolution, *Nat. Commun.*, 2020, **11**, 5075.
6 J. Li, L. Kong, Z. Wu, S. Zhang, X. Yang, J. Sha and G. Liu, Polydopamine-assisted construction of cobalt phosphide encapsulated in N-doped carbon porous polyhedrons for enhanced overall water splitting, *Carbon*, 2019, **145**, 694–700.
7 Z. Wu, Y. Zhao, W. Jin, B. H. Jia, J. Wang and T. Y. Ma, Recent Progress of Vacancy Engineering for Electrochemical Energy Conversion Related Applications, *Adv. Funct. Mater.*, 2021, **31**, 2009070.
8 H. Jing, P. Zhu, X. Zheng, Z. Zhang, D. Wang and Y. Li, Theory-oriented screening and discovery of advanced energy transformation materials in electrocatalysis, *Adv. Powder Mater.*, 2021, DOI: 10.1016/j.apmate.2021.10.004.
9 P. F. Cheng, T. Feng, Z. W. Liu, D. Y. Wu and J. Yang, Laser-direct-writing of 3D self-supported NiS_2/MoS_2 heterostructures as an efficient electrocatalyst for hydrogen evolution reaction in alkaline and neutral electrolytes, *Chin. J. Catal.*, 2019, **40**, 1147–1152.

10 H. Chen, X. Liang, Y. Liu, X. Ai, T. Asefa and X. Zou, Active site engineering in porous electrocatalysts, *Adv. Mater.*, 2020, **32**, 2002435.
11 J. Wang, Z. Zhang, H. Song, B. Zhang, J. Liu, X. Shai and L. Miao, Water Dissociation Kinetic–Oriented Design of Nickel Sulfides via Tailored Dual Sites for Efficient Alkaline Hydrogen Evolution, *Adv. Funct. Mater.*, 2021, **31**, 2008578.
12 X. P. Sun, Ni foam-supported NiCoP nanosheets as bifunctional electrocatalysts for efficient overall water splitting, *Chin. J. Catal.*, 2019, **40**, 1405–1407.
13 M. Zhao, W. Li, J. Y. Li, W. H. Hu and C. M. Li, Strong electronic interaction enhanced electrocatalysis of metal sulfide clusters embedded metal–organic framework ultrathin nanosheets toward highly efficient overall water splitting, *Adv. Sci.*, 2020, **7**, 2001965.
14 Q. Liu, J. Tian, W. Cui, P. Jiang, N. Cheng, A. M. Asiri and X. Sun, Carbon nanotubes decorated with CoP nanocrystals: a highly active non-noble-metal nanohybrid electrocatalyst for hydrogen, Evol., *Angew. Chem., Int. Ed.*, 2014, **53**, 6710–6714.
15 X. Li, L. Yang, T. Su, X. Wang, C. Sun and Z. Su, Graphene-coated hybrid electrocatalysts derived from bimetallic metal–organic frameworks for efficient hydrogen generation, *J. Mater. Chem. A*, 2017, **5**, 5000–5006.
16 C. T. Dinh, A. Jain, F. P. G. de Arquer, P. De Luna, J. Li, N. Wang, X. Zheng, J. Cai, B. Z. Gregory, O. Voznyy, B. Zhang, M. Liu, D. Sinton, E. J. Crumlin and E. H. Sargent, Multi-site electrocatalysts for hydrogen evolution in neutral media by destabilization of water molecules, *Nat. Energy*, 2018, **4**, 107–114.
17 Z. Chen, X. Duan, W. Wei, S. Wang and B. J. Ni, Recent advances in transition metal based electrocatalysts for alkaline hydrogen evolution, *J. Mater. Chem. A*, 2019, **7**, 14971–15005.
18 J. Sun, W. Xu, C. Lv, L. Zhang, M. Shakouri, Y. Peng, Q. Wang, X. Yang, D. Yuan, M. Huang, Y. Hu, D. Yang and L. Zhang, Co/MoN hetero-interface nanoflake array with enhanced water dissociation capability achieves the Pt-like hydrogen evolution catalytic performance, *Appl. Catal., B*, 2021, **286**, 119882.
19 B. Liu, Y. F. Zhao, H. Q. Peng, Z. Y. Zhang, C. K. Sit, M. F. Yuen, T. R. Zhang, C. S. Lee and W. J. Zhang, Nickel-cobalt diselenide 3D mesoporous nanosheet networks supported on Ni foam: an all-pH highly efficient integrated electrocatalyst for hydrogen evolution, *Adv. Mater.*, 2017, **29**, 1606521.
20 J. Y. Zhang, Y. Yan, B. Mei, R. Qi, T. He, Z. Wang, W. Fang, S. Zaman, Y. Su, S. Ding and B. Y. Xia, Local spin-state tuning of cobalt–iron selenide nanoframes for the boosted oxygen evolution, *Energy Environ. Sci.*, 2021, **14**, 365–373.
21 Q. Shi, C. Zhu, D. Du and Y. Lin, Robust noble metal-based electrocatalysts for oxygen evolution reaction, *Chem. Soc. Rev.*, 2019, **48**, 3181–3192.
22 H. Sun, W. Zhang, J.-G. Li, Z. Li, X. Ao, K.-H. Xue, K. K. Ostrikov, J. Tang and C. Wang, Rh-engineered ultrathin NiFe-LDH nanosheets enable highly-efficient overall water splitting and urea electrolysis, *Appl. Catal., B*, 2021, **284**, 119740.
23 L. Bao, S. Zhu, Y. Chen, Y. Wang, W. Meng, S. Xu, Z. Lin, X. Li, M. Sun and L. Guo, Anionic defects engineering of Co_3O_4 catalyst for toluene oxidation, *Fuel*, 2022, **314**, 122774.
24 Z. Wu, Y. Zhao, H. Wu, Y. Gao, Z. Chen, W. Jin, J. Wang, T. Ma and L. Wang, Corrosion Engineering on Iron Foam toward Efficiently Electrocatalytic Overall Water Splitting Powered by Sustainable Energy, *Adv. Funct. Mater.*, 2021, **31**, 2010437.
25 T. Zhang, B. Zhang, Q. Peng, J. Zhou and Z. M. Sun, Mo_2B_2 MBene-supported single-atom catalysts as bifunctional HER/OER and OER/ORR electrocatalysts, *J. Mater. Chem. A*, 2021, **9**, 433–441.
26 F. Zhang, R. Ji, Y. Liu, Y. Pan, B. Cai, Z. Li, Z. Liu, S. Lu, Y. Wang, H. Jin, C. Ma and X. Wu, A novel nickel-based honeycomb electrode with microtapered holes and abundant multivacancies for highly efficient overall water splitting, *Appl. Catal., B*, 2020, **276**, 119141.
27 Y. Liu, Q. Feng, W. Liu, Q. Li, Y. Wang, B. Liu, L. Zheng, W. Wang, L. Huang, L. Chen, X. Xiong and Y. Lei, Boosting interfacial charge transfer for alkaline hydrogen evolution via rational interior Se modification, *Nano Energy*, 2021, **81**, 105641.
28 D. Guo, J. Wang, L. Zhang, X. Chen, Z. Wan and B. Xi, Strategic Atomic Layer Deposition and Electrospinning of Cobalt Sulfide/Nitride Composite as Efficient Bifunctional Electrocatalysts for Overall Water Splitting, *Small*, 2020, **6**, e2002432.
29 W. Li, Y. Liu, M. Wu, X. Feng, S. A. T. Redfern, Y. Shang, X. Yong, T. Feng, K. Wu, Z. Liu, B. Li, Z. Chen, J. S. Tse, S. Lu and B. Yang, Carbon-Quantum-Dots-Loaded Ruthenium Nanoparticles as an Efficient Electrocatalyst for Hydrogen Production in Alkaline Media, *Adv. Mater.*, 2018, **30**, 1800676.
30 Y. Liu, X. Li, Q. Zhang, W. Li, Y. Xie, H. Liu, L. Shang, Z. Liu, Z. Chen, L. Gu, Z. Tang, T. Zhang and S. Lu, *Angew. Chem.*, 2021, **283**, 119583.
31 B. B. Yang, J. Y. Xu, D. Bin, J. Wang, J. Z. Zhao, Y. X. Liu, B. X. Li, X. N. Fang, Y. Liu, L. Qiao, L. F. Liu and B. H. Liu, Amorphous phosphatized ruthenium-iron bimetallic nanoclusters with Pt-like activity for hydrogen evolution reaction, *Appl. Catal., B*, 2021, **414**, 128784.
32 W. S. Fang, L. Huang, S. Zaman, Z. Wang, Y. J. Han and B. Y. Xia, *Chem. Res. Chin. Univ.*, 2020, **36**, 611–621.
33 W. B. Chen, C. S. Wang, S. B. Sua, H. Wang and D. D. Cai, Synthesis of ZIF-9(III)/Co LDH layered composite from ZIF-9(I) based on controllable phase transition for enhanced electrocatalytic oxygen evolution reaction, *Chem. Eng. J.*, 2021, **414**, 128784.
34 D. Gao, R. Liu, J. Biskupek, U. Kaiser, Y.-F. Song and C. Streb, Modular design of noble-metal-free mixed metal oxide electrocatalysts for complete water splitting, *Angew. Chem., Int. Ed.*, 2019, **58**, 4644.
35 R. Atchudan, T. N. Jebakumar Immanuel Edison, S. Perumal, R. Vinodh, N. Muthuchamy and Y. R. Lee, One-

pot synthesis of Fe_3O_4@graphite sheets as electrocatalyst for water electrolysis, *Fuel*, 2020, **277**, 118235.

36 S. J. Liu, J. Zhu, M. Sun, Z. X. Ma, K. Hu, T. Nakajima, X. H. Liu, P. Schmuki and L. Wang, Promoting Hydrogen Evolution Reaction through Oxygen Vacancies and Phase Transformation Engineering on Layered Double Hydroxide Nanosheets, *J. Mater. Chem. A*, 2020, **8**, 2490–2497.

37 X. L. Luo, Q. Shao, Y. C. Pi and X. Q. Huang, Trimetallic Molybdate Nanobelts as Active and Stable Electrocatalysts for the Oxygen Evolution Reaction, *ACS Catal.*, 2019, **9**, 1013–1018.

38 X. Zhao, H. T. Zhang, Y. Yan, J. H. Cao, X. Q. Li, S. M. Zhou, Z. M. Peng and J. Zeng, Engineeringthe Electrical Conductivity of Lamellar Silver-Doped Cobalt(II) Selenide Nanobelts for Enhanced Oxygen Evolution, *Angew. Chem., Int. Ed.*, 2017, **56**, 328–332.

39 C. Q. Huang, L. Yu, W. Zhang, Q. Xiao, J. Q. Zhou, Y. L. Zhang, P. F. An, J. Zhang and Y. Yu, N-doped Ni-Mo based sulfides for high-efficiency and stable hydrogen evolution reaction, *Appl. Catal., B*, 2020, **276**, 119137.

40 Z. H. Yan, H. M. Sun, X. Chen, H. H. Liu, Y. R. Zhao, H. X. Li, W. Xie, F. Y. Cheng and J. Chen, Anion insertion enhanced electrodeposition of robust metal hydroxide/oxide electrodes for oxygen evolution, *Nat. Commun.*, 2018, **9**, 2373.

41 C. H. Zhao, N. Li, R. Z. Zhang, Z. Q. Zhu, J. H. Lin, K. F. Zhang and C. J. Zhao, Surface Reconstruction of $La_{0.8}Sr_{0.2}Co_{0.8}Fe_{0.2}O_{3-\delta}$ for Superimposed OER Performance, *ACS Appl. Mater. Interfaces*, 2019, **11**, 47858–47867.

42 C. Zhao, P. Li, D. Shao, R. Zhang, S. Wang, Z. Zhu and C. Zhao, Phytic Acid-derived $Co_{2-x}Ni_xP_2O_7$-C/RGO and its Superior OER Electrocatalytic Performance, *Int. J. Hydrogen Energy*, 2019, **44**, 844–852.

43 L. Zhang, W. H. He, X. Xiang, Y. Li and F. Li, Roughening of windmill-shaped spinel Co_3O_4 microcrystals grown on a flexible metal substrate by a facile surface treatment to enhance their performance in the oxidation of water, *RSC Adv.*, 2014, **4**, 43357.

44 L. Li, G. W. Zhang, B. Wang and S. C. Yang, Constructing the Fe/Cr double (oxy)hydroxides on Fe_3O_4 for Boosting the Electrochemical Oxygen Evolution in Alkaline Seawater and Domestic Sewage, *Appl. Catal., B*, 2022, **302**, 120847.

45 H. Zhang, Y. Zhao, Y. Zhang, M. Zhang, M. Cheng, J. Yu, H. Liu, M. Ji, C. Zhu and J. Xu, Fe_3O_4 encapsulated in porous carbon nanobowls as efficient oxygen reduction reaction catalyst for Zn-air batteries, *Chem. Eng. J.*, 2019, **375**, 122058.

46 L. Wang, Q. Zhou, Z. H. Pu, Q. Zhang, X. Q. Mu, H. Y. Jing, S. L. Liu, C. Y. Chen and S. C. Mu, Surface Reconstruction Engineering of Cobalt Phosphides by Ru Inducement to form Hollow Ru-RuPx-CoxP Pre-electrocatalysts with Accelerated Oxygen Evolution Reaction, *Nano Energy*, 2018, **53**, 270–276.

47 N. L. W. Septiani, Y. V. Kaneti, K. B. Fathoni, Y. Guo, Y. Ide, B. Yuliarto, X. Jiang, H. K. Nugraha, D. Dipojono and Y. Y. Golberg, Tailorable nanoarchitecturing of bimetallic nickel–cobalt hydrogen phosphate via the self-weaving of nanotubes for efficient oxygen evolution, *J. Mater. Chem. A*, 2020, **8**, 3035–3047.

48 Y. Zhang, Q. Shao, S. Long and X. Q. Huang, Cobalt-molybdenum nanosheet arrays as highly efficient and stable earth-abundant electrocatalysts for overall water splitting, *Nano Energy*, 2018, **45**, 448–455.

49 Y. S. Jin, S. L. Huang, X. Yue, H. Y. Du and P. K. Shen, Mo- and Fe-Modified $Ni(OH)_2$/NiOOH Nanosheets as Highly Active and Stable Electrocatalysts for Oxygen Evolution Reaction, *ACS Catal.*, 2018, **8**, 2359–2363.

50 P. X. Ji, X. Luo, D. Chen, H. H. Jin, Z. H. Pu, W. H. Zeng, J. W. He, H. W. Bai, Y. C. Liao and S. C. Mu, Significantly Improved Water Oxidation of CoP Catalysts by Electrochemical Activation, *ACS Sustainable Chem. Eng.*, 2020, **8**, 17851–17859.

51 S. Z. Chen, Y. Zhang, J. Jin, H. X. Qu, T. L. Zhu and Q. Zhong, 3D network Ni-based electrocatalysts with interfacial active sites of Ru QDs and $Ni(OH)_2$ for efficient hydrogen evolution reaction under large current density in alkaline environment, *Electrochim. Acta*, 2020, **356**, 136732.

52 X. J. Zhai, Q. P. Yu, G. S. Liu, J. L. Bi, Y. Zhang, J. Q. Chi, J. P. Lai, B. Yang and L. Wang, Hierarchical microsphere MOF arrays with ultralow Ir doping for efficient hydrogen evolution coupled with hydrazine oxidation in seawater, *J. Mater. Chem. A*, 2021, **9**, 27424.

53 L. B. Wu, L. Yu, F. H. Zhang, B. McElhenny, D. Luo, A. Karim, S. Chen and Z. F. Ren, Heterogeneous Bimetallic Phosphide Ni_2P-Fe_2P as an Efficient Bifunctional Catalyst for Water/Seawater Splitting, *Adv. Funct. Mater.*, 2020, **31**, 2006484.

54 J. C. Li, C. Zhang, C. Zhang, H. J. Ma, Y. Yang, Z. Q. Guo, Y. Y. Wang and H. X. Ma, Electronic configuration of single ruthenium atom immobilized in urchin-like tungsten trioxide towards hydrazine oxidation-assisted hydrogen evolution under wide pH media, *Chem. Eng. J.*, 2022, **430**, 132953.

55 H. G. Liu, Z. Hu, Q. L. Liu, P. Sun, Y. F. Wang, S. L. Chou, Z. Z. Hu and Z. Q. Zhang, Single-atom Ru anchored in nitrogen-doped MXene (Ti3C2Tx) as an efficient catalyst for the hydrogen evolution reaction at all pH values, *J. Mater. Chem. A*, 2020, **8**, 24710–24717.

56 Y. L. Wu, X. F. Li, Y. S. Wei, Z. M. Fu, W. B. Wei, X. T. Wu, Q. L. Zhu and Q. Xu, Ordered Macroporous Superstructure of Nitrogen-Doped Nanoporous Carbon Implanted with Ultrafine Ru Nanoclusters for Efficient pH-Universal Hydrogen Evolution Reaction, *Adv. Mater.*, 2021, **33**, 2006965.

57 S. J. Liu, Y. J. Chen, L. Yu, Y. Lin, Z. Liu, M. M. Wang, Y. J. Chen, C. Zhang, Y. Pan, Y. Q. Liu and C. G. Liu, A supramolecular-confinement pyrolysis route to ultrasmall rhodium phosphide nanoparticles as a robust electrocatalyst for hydrogen evolution in the entire pH range and seawater electrolysis, *J. Mater. Chem. A*, 2020, **8**, 25768–25779.

58 L. Tang, J. J. Yu, Y. Zhang, Z. Z. Tang and Y. Qin, Boosting the Hydrogen Evolution Reaction Activity of Ru in Alkaline and Neutral Media by Accelerating Water Dissociation, *RSC Adv.*, 2021, **11**, 6107.

59 S. Drouet, J. Creus, V. Collière, C. Amiens, J. García-Antón, X. Sala and K. Philippot, A porous Ru nanomaterial as an efficient electrocatalyst for the hydrogen evolution reaction under acidic and neutral conditions, *Chem. Commun.*, 2017, **53**, 11713.

60 F. L. Yang, Y. M. Zhao, Y. S. Du, Y. T. Chen, G. Z. Cheng, S. L. Chen and W. Luo, A Monodisperse Rh_2P-Based Electrocatalyst for Highly Efficient and pH-Universal Hydrogen Evolution Reaction, *Adv. Energy Mater.*, 2018, **8**, 1703489.

61 Z. H. Pu, I. S. Amiinu, Z. K. Kou, W. Q. Li and S. C. Mu, RuP_2-Based Catalysts with Platinum-like Activity and Higher Durability for the Hydrogen Evolution Reaction at All pH Values, *Angew. Chem., Int. Ed.*, 2017, **56**, 11559.

62 X. Y. Zhang, F. T. Li, R. Y. Fan, J. Zhao, B. Dong, F. L. Wang, H. J. Liu, J. F. Yu, C. G. Liu and Y. M. Chai, F, P double-doped Fe_3O_4 with abundant defect sites for efficient hydrogen evolution at high current density, *J. Mater. Chem. A*, 2021, **9**, 15836–15845.

63 M. Zhu, Q. Yan, Y. Q. Xue, Y. D. Yan, K. Zhu, K. Ye, J. Yan, D. X. Cao, H. J. Xie and G. L. Wang, Free-Standing P-Doped $NiSe_2/MoSe_2$ Catalyst for Efficient Hydrogen Evolution in Acidic and Alkaline Media, *ACS Sustainable Chem. Eng.*, 2022, **10**, 279–287.